

Quantumness and entropic uncertainty for a pair of static Unruh-DeWitt detectors

Yu-Kun Zhang,¹ Tariq Aziz,¹ Li-Juan Li,¹ Xue-Ke Song,¹ Liu Ye,¹ and Dong Wang^{1,*}

¹*School of Physics & Optoelectronic Engineering, Anhui University, Hefei 230601, People's Republic of China*
(Dated: March 7, 2025)

In this study, we investigate a pair of detectors operating in Minkowski space-time and analyze the characteristics of various quantum resources within this framework. Specifically, we focus on examining the properties of Bell nonlocality, quantum coherence, the nonlocal advantage of quantum coherence (NAQC), and measured uncertainty in relation to the energy ratio and the distance between the detectors. Additionally, we examine how the initial states influence these quantum properties. Notably, our findings reveal that both a larger energy ratio and a greater separation between the detectors degrade the system's quantumness. Moreover, we explore the evolution of entropic uncertainty and demonstrate its inverse correlation with both Bell nonlocality and coherence, highlighting the intricate interplay between these quantum resources. These insights provide a deeper understanding of quantumness in a relativistic framework and may contribute to the ongoing discussion on the black hole information paradox.

I. INTRODUCTION

As an emerging discipline, quantum information science integrates quantum physics and information theory, leveraging the former to investigate the fundamental nature of reality at low temperatures and on microcosmic scales, while the latter provides a framework for information processing. The core concept of quantum information theory is the qubit [1, 2]. Unlike classical bits, which exist solely in the states 0 or 1, qubits can exist in a superposition of $|0\rangle$ and $|1\rangle$ simultaneously. This property enables quantum computing to offer potential advantages over classical computing for certain computational tasks [3, 4].

Quantum nonlocality refers to the phenomenon in which two spatially separated entangled particles exhibit correlated behaviors, such that a measurement performed on one particle instantaneously influences the state of the other. This instantaneous effect contradicts the principles of local realism. To address this issue, Bell introduced the concept of Bell's inequality [5], demonstrating that its violation provides evidence for the existence of nonclassical quantum correlations. Building on this foundation, researchers later developed the Clauser-Horne-Shimony-Holt (CHSH) inequality to further explore and test quantum nonlocality [6–9]. This demonstrates the maximum achievable violation of these limits. These advancements have further refined the theoretical framework of quantum mechanics, providing deeper insights into quantum entanglement and its implications.

Quantum resources, including entanglement and coherence [10–13], are considered as crucial aspects in the region of quantum information processing. Quantum coherence, which arises from quantum superposition, plays a key role in quantum mechanics. It has evolved alongside advancements in quantum optics and quantum computing [14, 15], with becoming emerging as its most prominent application. To quantify coherence, several promising methods have been proposed, such as the l_1 -norm coherence [16–18] and the relative entropy of coherence [19, 20]. In classical physics, local real-

ism is regarded as an objective principle; however, in quantum physics, this principle can be violated.

Another important quantum resource is called as the steerability of local coherence, which is formulated as a game between Alice and Bob based on coherence complementarity relations [21]. For a two-qubit state $\hat{\rho}_{AB}$, local measurements on subsystem A , followed by classical communication, allow the average coherence of subsystem B 's conditional state to exceed the single-qubit coherence limit in mutually unbiased bases. As a result, the conditional state of subsystem B can achieve a nonlocal advantage of quantum coherence (NAQC).

In the study of quantum systems, uncertainty serves as a fundamental tool for evaluating their states. In quantum information theory, the entropic uncertainty relation is frequently used to depict the system's uncertainty. In recent years, this relation has been extensively explored across various fields [22–28], and its connections with other quantum resources have been investigated [29–42], thereby deepening our understanding of the quantum world.

On the other hand, general relativity describes gravity as a geometric property of space time, and many of its theoretical predictions have been gradually confirmed. Although quantum information and relativity originate from distinct domains, namely, the microscopic and macroscopic worlds, intriguing connections exist between the two fields. Notable examples include quantum field theory (QFT) [43], relativistic quantum entanglement [44, 45], and the black-hole information paradox [46–48]. Consequently, the investigation of relativistic quantum information has attracted growing interest in recent years.

To explore relativistic quantum information, a pair of two-level atoms, known as the Unruh-DeWitt detectors [49–53], has been extensively studied. In general, such detector pairs are employed to investigate Bell nonlocality, coherence, the nonlocal advantage of quantum coherence, and entropic uncertainty in the presence of a vacuum scalar field. In this study, we assume that the two detectors interact independently with the vacuum field they occupy. For simplicity, the interaction is modeled as a monopole coupling. To avoid complications arising from motion, we assume that both detectors remain static indefinitely and that their interaction with the field is permanent. This model is particularly significant for under-

* dwang@ahu.edu.cn

standing the black hole information paradox, as a Minkowski observer is equivalent to a freely falling observer in black hole space–time. All results presented in this study are derived using second-order perturbative approximations.

The remainder of this paper is structured as follows. In Section II, we provide a detailed description of the model employed in this study. Section III explores various aspects of quantumness, including nonlocality, coherence, and uncertainty. Finally, we conclude the paper with a summary of our findings.

II. MODEL

Detector models are commonly employed to extract relativistic quantum information. We consider a pair of two-level detectors, referred to as Alice and Bob, with energy-level gaps given by $\Delta E_j = E_{1_j} - E_{0_j}$ where j corresponds to A and B . We prepare this pair of detectors in an entangled state, which can be expressed as

$$|\phi\rangle = \sin\theta|0_A0_B\rangle + \cos\theta|1_A1_B\rangle, \quad (1)$$

where $\sin\theta$ and $\cos\theta$ are state parameters; and $|0\rangle$ and $|1\rangle$ denote the ground and excited states of the detectors, respectively. The detectors are placed in $(3+1)$ -dimensional Minkowski space–time, with their trajectories defined as

$$\begin{aligned} t_A &= \tau_A, & t_B &= \tau_B, \\ \mathbf{X}_A &= 0, & \mathbf{X}_B &= \mathbf{d}, \end{aligned} \quad (2)$$

where τ_j denotes the proper time of the j -th detector, and \mathbf{d} is a constant vector representing the distance between the two detectors. Additionally, the interaction between the detectors and the real scalar field $\phi(x)$ is modeled as a monopole coupling, which can be expressed as follows:

$$S_{int} = \sum_{i=A,B} \nu_j \int d\tau_j \kappa_j m_j(j) \phi(x_j(\tau_j)), \quad (3)$$

where ν_i is the coupling constant, and $m_j(\tau_j)$ represents the monopole operator of the i th detector, which can be expressed as:

$$m_j(\tau_j) = e^{iH_j\tau_j} (|0_j\rangle\langle 1_j| + |1_j\rangle\langle 0_j|) e^{-iH_j\tau_j}. \quad (4)$$

For the j -th detector, H_j denotes the free Hamiltonian, while the switching function κ_j governs the interaction duration. The initial composite state of the detector-field system can be expressed as $|\Psi\rangle = |0_M\rangle \otimes |\psi\rangle$, where $|0_M\rangle$ denotes the real scalar field in the vacuum state and the detector system in Minkowski space–time. By tracing out the field's degrees of freedom, we obtain the initial density matrix of the detector system as follows:

$$\hat{\rho}_{AB}(t_0) = \begin{pmatrix} \sin^2\theta & 0 & 0 & \sin\theta\cos\theta \\ 0 & 0 & 0 & 0 \\ 0 & 0 & 0 & 0 \\ \cos\theta\sin\theta & 0 & 0 & \cos^2\theta \end{pmatrix}. \quad (5)$$

During the interaction of a real scalar field, the evolution of the composite system can be written as follows:

$$\begin{aligned} \hat{\rho}_{AB}(t) &= \text{Tr}_\psi \left(\hat{T} e^{iS_{int}} |\Psi\rangle \langle \Psi| \hat{T} e^{iS_{int}} \right) \\ &= \begin{pmatrix} \rho_{11} & 0 & 0 & \rho_{14} \\ 0 & \rho_{22} & \rho_{23} & 0 \\ 0 & \rho_{32} & \rho_{33} & 0 \\ \rho_{41} & 0 & 0 & \rho_{44} \end{pmatrix}, \end{aligned} \quad (6)$$

where \hat{T} denotes the time-ordering operator. The explicit forms of the density matrix above are presented in Ref. [11].

Because both detectors are identical, their energy gaps satisfy $\Delta E_A = \Delta E_B \equiv \Delta E$, and their coupling constants satisfy $\nu_A = \nu_B \equiv \nu$. We assume that the interaction duration is an adiabatic process, allowing the switching function κ_j to be set to unity. Consequently, the elements of the evolved density matrix $\hat{\rho}_{AB}$ reduce to the following forms:

$$\begin{aligned} \rho_{11} &= \cos^2\theta \left(1 - \nu^2 P_A'' - \nu^2 P_B'' \right), \\ \rho_{22} &= \cos^2\theta \nu^2 P_B'', \\ \rho_{33} &= \cos^2\theta \nu^2 P_A'', \\ \rho_{44} &= \sin^2\theta, \\ \rho_{14} &= \sin\theta \cos\theta \left(1 - \nu^2 M_A - \nu M_B \right), \\ \rho_{23} &= \cos^2\theta \nu^2 \Re_{AB}, \\ \rho_{32} &= \cos^2\theta \nu^2 \Re_{AB}^*, \\ \rho_{41} &= \sin\theta \cos\theta \left(1 - \nu^2 M_A^* - \nu^2 M_B^* \right), \end{aligned} \quad (7)$$

where

$$\begin{aligned} P_j''(\Delta E) &= \int \int d\tau_j d\tau'_j e^{-i\Delta E(\tau_j - \tau'_j)} G_W(x'_j, x_j), \\ M_j(\Delta E) &= \int \int d\tau_j d\tau'_j e^{-i\Delta E(\tau_j - \tau'_j)} \Theta(\tau_j - \tau'_j) \\ &\quad * (G_W(x'_j, x_j) + G_W(x_j, x'_j)), \\ \Re_{AB}(\Delta E) &= \int \int d\tau_A d\tau'_B e^{i\Delta E(\tau'_B - \tau_A)} G_W(x'_B, x_A), \end{aligned} \quad (8)$$

herein, $G_W(x'_j, x_j)$ represents the positive frequency Wightman function. In the above functions, $P_j(\Delta E)$ denotes the transition probability of the j -th ($j \in \{A, B\}$) detector from the ground state to the excited state, which is entirely determined by the spontaneous emission probability. Additionally, $M_j(\Delta E)$ is determined by the expectation value of the anti-commutator of the external scalar field, while $\Re_{AB}(\Delta E)$ represents the interaction between the field and detectors. Moreover, $G_W(x'_j, x_j) + G_W(x_j, x'_j)$ the term in second equation of Eq. (8) can be computed as $\langle 0_M | \{ \phi(x'_j), \phi(x_j) \} | 0_M \rangle$.

By integrating Eq. (8), we obtain

$$\begin{aligned} P_j'' &= \frac{\delta(0)}{2c^3} \sqrt{\Delta F}, \\ \text{Re}(M_j) &= \frac{\delta(0)}{4c^3} \sqrt{\Delta F}, \\ \Re_{AB} &= \frac{\delta(0)}{2c^3} \sqrt{\Delta F} \frac{\sin\left(\frac{d}{c} \sqrt{\Delta F}\right)}{\left(\frac{d}{c} \sqrt{\Delta F}\right)}, \end{aligned} \quad (9)$$

where $\Delta F = (\Delta E^2 - (mc^2)^2)/(mc^2)^2$ represents the energy ratio between the detector and the external field, effectively capturing the energy difference between them; Re denotes the real part of the equation; d represents the distance between the two detectors; and c represents the velocity of light in Minkowski space-time. Additionally, $\delta(0)$ is the Dirac delta function, arising from the infinite time integration, and can be expressed as:

$$\delta(0) = \lim_{T \rightarrow \infty} \frac{1}{2\pi} \int_{-T/2}^{T/2} du. \quad (10)$$

It is evident that the Dirac delta function diverges. Generally, computations of the relevant quantities are more convenient when the function is convergent. Because the $\delta(0)$ function is independent of the other components except for time T , we can evaluate [11] the quantum resources considered here by

$$\begin{aligned} \dot{\xi} &= \frac{\xi}{T} = (\text{finite quantity}) \times \frac{\delta(0)}{T} \\ &= (\text{finite quantity}) \times \lim_{T \rightarrow \infty} \frac{1}{2\pi T} \int_{-T/2}^{T/2} du, \end{aligned} \quad (11)$$

where ξ represents the quantum resources under consideration, including Bell nonlocality, coherence, NAQC, quantum uncertainty, and the integral in Eq. (11) can be calculated using the result for $\frac{1}{2\pi}$.

III. QUANTUM CORRELATION AND ENTROPIC UNCERTAINTY

In this section, we first review Bell nonlocality and explore its dynamical evolution within the proposed model. Subsequently, we analyze two types of quantum coherence, namely, l_1 -norm coherence and relative entropy coherence, demonstrating how the system's coherence evolves over time. Building on these measures, we investigate the nonlocal advantage of quantum coherence, assess state properties through this nonlocal advantage, and compare the characteristics of the nonlocal advantages of the two types of coherence. Finally, we explore quantum uncertainty within this framework and reveal its relationship with the aforementioned quantum resources.

A. Bell nonlocality

Bell introduced the concept of Bell's inequality to analyze local realism and hidden variables [5]. A quantum

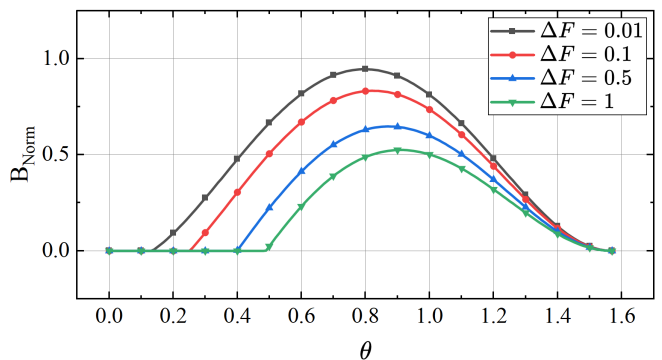


FIG. 1. The Bell nonlocality $B_{\text{Norm}}(\hat{\rho}_{AB})$, as a function of the state parameter θ with different energy ratios $\Delta F = 0.01, 0.1, 0.5, 1$ for a pair of detectors in Minkowski space-time. Here, the parameters $c = d = m = 1$ are set.

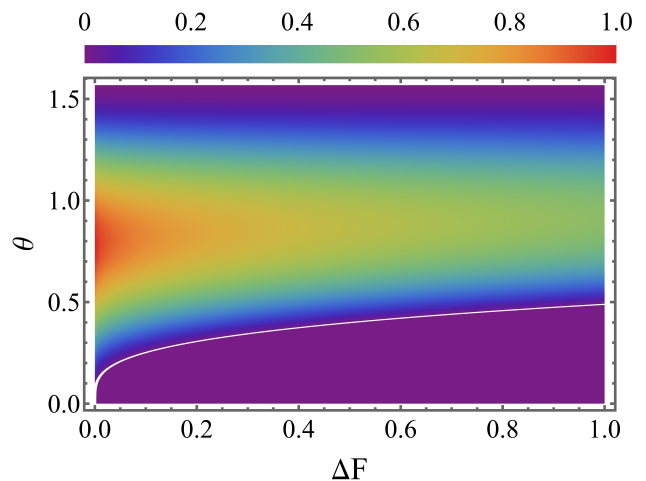


FIG. 2. The Bell nonlocality $B_{\text{Norm}}(\hat{\rho}_{AB})$ as a function of the state parameter θ and the energy ratio ΔF . The white line represents the boundary distinguishing states with and without Bell nonlocality. Specifically, the regions below the white line correspond to states that do not exhibit quantum nonlocality. Here, the parameters $c = d = m = 1$ are set.

system comprising of Alice and Bob can be represented as $\frac{1}{\sqrt{2}}(|01\rangle - |10\rangle)$ where measurements are performed using the bases $x(y)$. The outcomes of these measurements follow a conditional probability distribution, $p(ab|xy) \neq p(a|x)p(b|y)$, indicating that the measurement results are not independent. Consequently, if we consider all variables that would make the inequality false, the conditional probability distribution can be written as:

$$p(ab|xy, \lambda) = p(a|x, \lambda) p(b|y, \lambda), \quad (12)$$

where λ represents a set of hidden variables associated with each measurement, satisfying the normalization condition $\int d\lambda q(\lambda) \equiv 1$. Consequently, the conditional probability distribution can be expressed as:

$$p(ab|xy, \lambda) = \int d\lambda q(\lambda) p(a|x, \lambda) p(b|y, \lambda). \quad (13)$$

In a Bell experiment, Alice and Bob perform different measurements, $x, y \in \{0, 1\}$, and the corresponding outcomes are $a, b \in \{-1, +1\}$, so the expectation value of the measurements x and y are defined as follows:

$$\langle a_x b_y \rangle = \sum_{a,b} ab p(ab|xy). \quad (14)$$

Further, consider the quantity $S = \langle a_0 b_0 \rangle + \langle a_0 b_1 \rangle + \langle a_1 b_0 \rangle - \langle a_1 b_1 \rangle$, which is a function of $p(ab|xy)$.

If these conditional probability distributions adhere to local constraints, the quantity S can be restrained in

$$S = \langle a_0 b_0 \rangle + \langle a_0 b_1 \rangle + \langle a_1 b_0 \rangle - \langle a_1 b_1 \rangle \leq 2. \quad (15)$$

This is the well-known Clauser-Horne-Shimony-Holt (CHSH) inequality.

The maximum violation of the CHSH inequality serves as an effective measure of Bell nonlocality; for a two qubit quantum system $\hat{\rho}_{AB}$, the maximum CHSH inequality violation can be written as

$$B_{\max}(\hat{\rho}_{AB}) = 2\sqrt{M_{AB}}, \quad (16)$$

where $M_{AB} = \max_{i < j} (m_i + m_j)$, $m_{i(j)}(i, j = 1, 2, 3)$ is the eigenvalue of matrix $\hat{T}^\dagger \hat{T}$, and \hat{T} is the correlation matrix. The analytical expressions $B_{\max}(\hat{\rho}_{AB})$ are presented in Appendix A.

Fig. 1 depicts the variation of Bell nonlocality with respect to the state parameter θ . Notably, the Bell nonlocality has been normalized, with its explicit expression provided in Appendix A. As observed, Bell nonlocality initially increases with the state parameter θ , before reaching a peak and subsequently decreasing.

Moreover, it is evident from Fig. 1 that not all states exhibit nonlocality in the current model. This observation raises an important question regarding which states are nonlocal and which remain local, a distinction that holds significance for practical quantum information processing. To address this, we plot the Bell nonlocality versus both the state parameter and the energy ratio ΔF in Fig. 2. Specifically, a boundary of states with and without Bell nonlocality was offered. Moreover, as the energy ratio continuously increases, the range of detectable states with nonlocality gradually diminishes.

B. l_1 -norm coherence and relative entropy of coherence

In quantum information science, quantum coherence is recognized as a fundamental quantum resource for practical information processing. Various quantification methods have been developed, including the l_1 -norm of coherence and relative entropy of coherence. Specifically, the l_1 -norm of coherence is widely employed due to its operational significance and computational feasibility. This measure is defined as the sum of the absolute values of the off-diagonal elements in the density matrix of a quantum state, capturing the degree of coherence among the system's eigenstates. Given a density matrix $\hat{\rho}$, the l_1 -norm coherence, on the basis of eigenvectors of

the Pauli spin observables $\hat{\sigma}_i$ ($i = x, y, z$), is expressed as the sum of the absolute values of its off-diagonal elements [13], which can be expressed as:

$$C_{l_1}^{\hat{\sigma}_i}(\hat{\rho}) = \sum_{R \neq S} \langle R | \hat{\rho} | S \rangle, \quad (17)$$

where $\{|R\rangle, |S\rangle\}$ represent the eigenvectors of $\hat{\sigma}_i$. For convenience, we select the $\hat{\sigma}_z$ Pauli spin observable as the reference basis for our calculation. These off-diagonal elements are closely related to the coherence of the system, reflecting the presence of quantum superposition. Consequently, a higher l_1 -norm coherence value indicates a greater degree of coherence within the quantum system.

Additionally, the relative entropy of coherence (REC) serves as an alternative and effective measure of quantum coherence in quantum information theory. This measure is derived from the relative entropy between quantum states, which quantifies the "distance" between two quantum states. REC characterizes the "degree of deviation" of the target quantum state from the incoherent state: the greater deviation, the stronger coherence. Mathematically, it is expressed as follows:

$$C_{\text{REC}}(\hat{\rho}) = S(\hat{\rho}_{\text{diag}}) - S(\hat{\rho}), \quad (18)$$

where $S(\hat{\rho}) = -\text{Tr}(\hat{\rho} \log \hat{\rho})$ denotes the von Neumann entropy, and ρ_{diag} is the non-coherence state with the density matrix consisting only of the diagonal elements.

To analyze coherence in the present framework, Fig. 3 illustrates the variation of the l_1 -norm coherence and REC with respect to the state parameter θ for different energy ratios. Several key observations can be made: (1) Both coherence measures initially increase and then decrease as the growing state parameter grows. (2) The maximum coherence for both measures occurs at $\theta = \pi/4$. (3) The l_1 -norm coherence consistently exceeds REC in this study. (4) The evolution of both coherence measures exhibits symmetry around $\theta = \pi/4$, particularly when the energy ratio is relatively small.

Next, we examine how the distance between the two detectors influences the system's coherence. Figs. 4 and 5 illustrate the dynamics of the l_1 -norm coherence and REC of the two detectors with respect to the distance between the two detectors for different energy ratios, considering the detectors are initially in a maximally entangled state. The key findings are as follows: (1) Both coherence measures decrease as the distance d increases, indicating that the distance can partially degrade the system's quantumness. (2) The two coherences will be frozen to fixed non-zero values for $d \rightarrow \infty$, confirming the persistence of nonlocality regardless of spatial separation between the two detectors. This behavior can be understood by analyzing the explicit expressions of the eigenstates of the density matrix, provided in Appendix B, which remain independent of distance d .

C. Nonlocal advantage of quantum coherence

Now, we briefly introduce the concept of the nonlocal advantage of quantum coherence (NAQC) based on the l_1 -norm

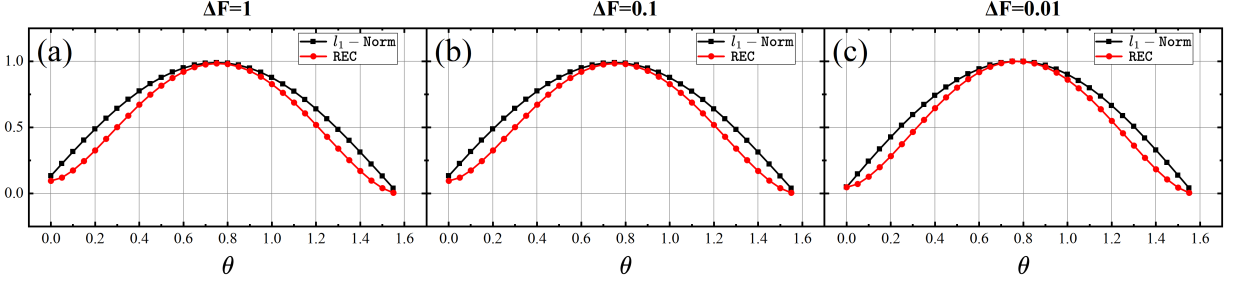


FIG. 3. Dynamics of l_1 -norm coherence (black line) and relative entropy coherence (red line) with the state parameter θ for various ΔF in Graphs (a)-(c). Graph (a): $\Delta F = 1$, Graph (b): $\Delta F = 0.1$, Graph (c): $\Delta F = 0.01$, where $c = d = m = 1$.

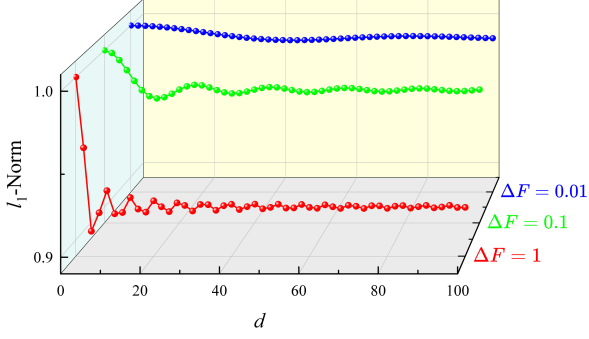


FIG. 4. Dynamics of l_1 -norm coherence with the distance d between two detectors. The energy ratio $\Delta F = 1$ (red), $\Delta F = 0.1$ (green), and $\Delta F = 0.01$ (blue). $\theta = \pi/4$ is set and corresponds to the maximal entanglement, and $c = m = 1$.

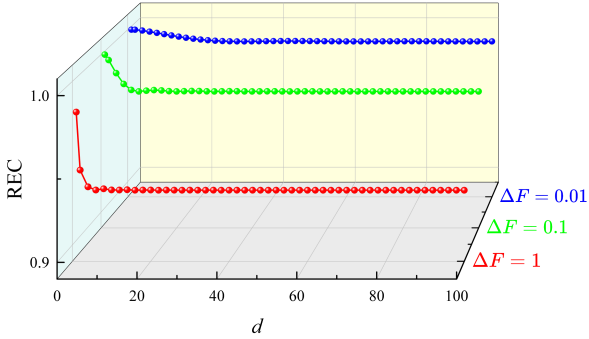


FIG. 5. Dynamics of relative entropy coherence with the distance d between two detectors. The energy ratio $\Delta F = 1$ (red), $\Delta F = 0.1$ (green), and $\Delta F = 0.01$ (blue). $\theta = \pi/4$ is set and corresponds to the maximal entanglement, and $c = m = 1$.

coherence and relative entropy of coherence (REC). In the previous section, we discuss the l_1 -norm coherence, as defined in Eq. (17). However, coherence is subject to an upper bound. For mutually unbiased bases, the complete complementarity relation of coherence should satisfy the following relation:

$$\sum_{i=x,y,z} C_{l_1}^{\hat{\sigma}_i} \leq C_{\max}, \quad (19)$$

which is a complementarity relation [21], where $C_{\max} =$

$\sqrt{6} \approx 2.45$ is the upper bound, independent of the quantum state. Equality in Eq. (19) is achieved for a specific pure state, $\hat{\rho}_{\max} = \frac{1}{2} \left[\frac{1}{\sqrt{3}} (\hat{\sigma}_x + \hat{\sigma}_y + \hat{\sigma}_z) + \hat{\mathbb{I}} \right]$, where $\hat{\mathbb{I}}$ represents the identity matrix.

To gain deeper insights into NAQC, one can conceptualize a game between Alice and Bob designed to demonstrate (NAQC). In this scenario, Alice and Bob each possesses qubits A and B , respectively, with the overall quantum state represented by $\hat{\rho}_{AB}$. At the start of the game, Alice randomly performs a measurement operation $\Pi_i^b = [\mathbb{I} + (-1)^b \hat{\sigma}_i] / 2$ on qubit A , where the value of b is zero or one. The probability of obtaining a given outcome from the measurement is given by $P_{\Pi_i^b} = \text{Tr}[(\Pi_i^b \otimes \mathbb{I}) \hat{\rho}_{AB}]$. Upon completing the measurement and recording the result, Alice must communicate her measurement choice and outcome to Bob. Using this information, Bob's task is to randomly measure the coherence of qubit B in the eigenbases of the two remaining Pauli operators, $\hat{\sigma}_j$ and $\hat{\sigma}_k$, excluding the operator $\hat{\sigma}_i$ that was chosen by Alice. To determine whether the game successfully demonstrates NAQC for qubit B , a specific criterion must be met. Specifically, the following quantity must be calculated:

$$\mathcal{N}^{l_1}(\hat{\rho}_{AB}) = \frac{1}{2} \sum_{i,j,k} P \left(\hat{\rho}_{\Pi_j^b \neq i}^b C_{l_1}^{\hat{\sigma}_i} \left(\hat{\rho}_{B|\Pi_j^b \neq i} \right) \right) \quad (20)$$

with l_1 -norm coherence, which uses an averaging method for all possible probabilities. If $\mathcal{N}^{l_1}(\hat{\rho}_{AB}) > C_{\max}^{l_1}$ holds, then we say that NAQC for qubit B is achieved.

Additionally, we also consider another form of nonlocal advantage based on the relative entropy of coherence. In this case, the complete complementarity relation and the nonlocal advantage through REC are given by [21]

$$\sum_{i=x,y,z} C_{\text{REC}}^{\hat{\sigma}_i} \leq C_2^m, \quad (21)$$

$$\mathcal{N}^{\text{REC}}(\hat{\rho}_{AB}) = \frac{1}{2} \sum_{i,j,k} P \left(\hat{\rho}_{\Pi_j^b \neq i}^b C_{\text{REC}}^{\hat{\sigma}_i} \left(\hat{\rho}_{B|\Pi_j^b \neq i} \right) \right). \quad (22)$$

where $C_2^m \approx 2.23$ represents the upper bound on the complementarity relation. Thus, the nonlocal advantage of REC is achieved when $\mathcal{N}^{\text{REC}}(\hat{\rho}_{AB}) > C_2^m$.

Here, the analytical expressions for the nonlocal advantage of quantum coherence are provided in Appendix C. Addition-

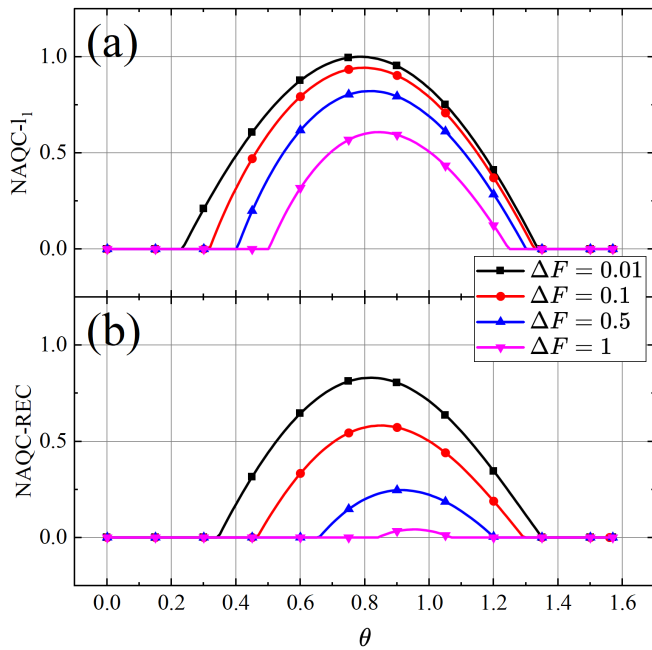


FIG. 6. Dynamics of the nonlocal advantage of quantum coherence with state parameter θ for a pair of detectors in Minkowski space-time. Graph (a): nonlocal advantage of l_1 -norm coherence. Graph (b): nonlocal advantage of relative entropy coherence. The parameters are set as $c = d = m = 1$ in the plots.

ally, for convenience, we define the normalized nonlocal advantage based on the l_1 -norm coherence and REC. To further explore the characteristics of NAQC, we plot the normalized nonlocal advantage of l_1 -norm coherence and REC with respect to the state parameter θ in Fig. 6. From our analysis, we conclude the following: (1) the existence of zero-valued NAQC, indicating that not all states exhibit the nonlocal advantage of quantum coherence in the current model. (2) A smaller energy ratio ΔF between the detector and field enhances the nonlocal advantage of quantum coherence, suggesting that a smaller gap between them is beneficial for maximizing the system's quantumness. (3) In general, the nonlocal advantage of l_1 -norm coherence exceeds that of REC, indicating that NAQC based on l_1 -norm coherence is more robust than that based on REC.

Next, we investigate the boundary of the states exhibiting NAQC by plotting the nonlocal advantages of the two types of coherence with respect to the state parameter θ in Fig. 7. As illustrated in the figure, the ranges of states exhibiting NAQC gradually shrinks as the energy ratio ΔF increases, and the maximum values of the nonlocal advantage decrease accordingly. Notably, compared to the nonlocal advantage of REC, the detectable range of the nonlocal advantage of l_1 -norm coherence is broader and less affected by the energy ratio. Thus, we argue that the nonlocal advantage of l_1 -norm coherence is more robust than that of REC, which aligns with our previous conclusions.

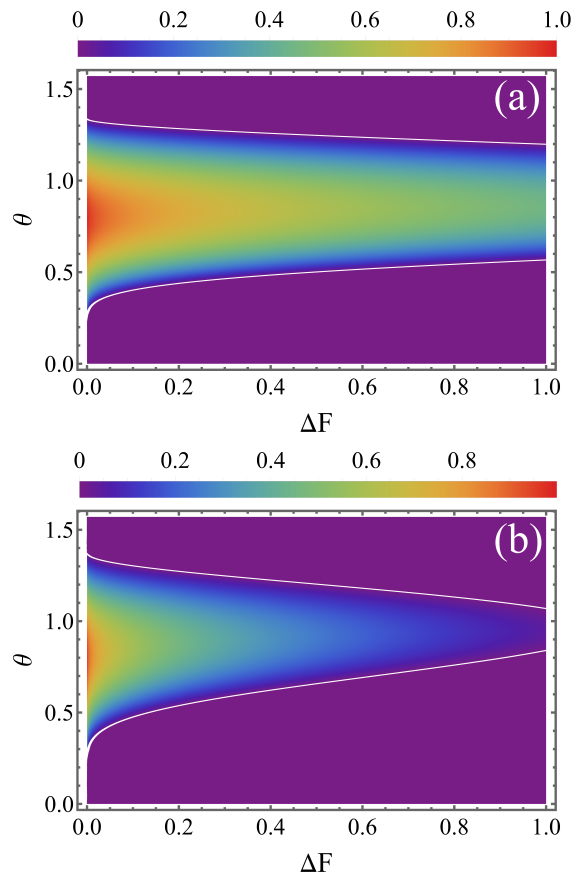


FIG. 7. Detectable state parameter range of nonlocal advantage of quantum coherence with change in energy ratio. Graph (a): Nonlocal advantage of l_1 -norm coherence. Graph (b): Nonlocal advantage of relative entropy of coherence. The white lines in both graphs signify the boundaries between states with and without NAQC. The parameters $c = d = m = 1$ are set.

D. Entropic uncertainty and lower bound

The entropic uncertainty relation (EUR) was first formulated by Deutsch [54], later refined by Karus [55], and rigorously by Maassen and Uffink [56]. It is expressed as

$$H(\hat{R}) + H(\hat{S}) \geq \log_2 \frac{1}{c} := q_{MU}, \quad (23)$$

where $H(X) = -\sum_k x_k \log_2 x_k$ denotes the Shannon entropy of the observable $X \in \{\hat{R}, \hat{S}\}$, x_k denotes the probability of obtaining outcome k , and q_{MU} denotes the incompatibility measure, defined as $c = \max_{i,j} |\langle \hat{r}_i | \hat{s}_j \rangle|^2$; here, $|\hat{r}_i\rangle$ and $|\hat{s}_j\rangle$ are the eigenstates of \hat{R} and \hat{S} , respectively. For composite quantum systems, Renes *et al* and Berta *et al* proposed quantum-memory-assisted entropic uncertainty relations (QMA-EUR) for arbitrary pairs of observables, which can be mathematically expressed as follows:

$$S(\hat{R}|B) + S(\hat{S}|B) \geq q_{MU} + S(A|B), \quad (24)$$

where $S(\hat{R}|B) = S(\hat{\rho}_{\hat{R}B}) - S(\hat{\rho}_B)$ and $S(\hat{S}|B) = S(\hat{\rho}_{\hat{S}B}) -$

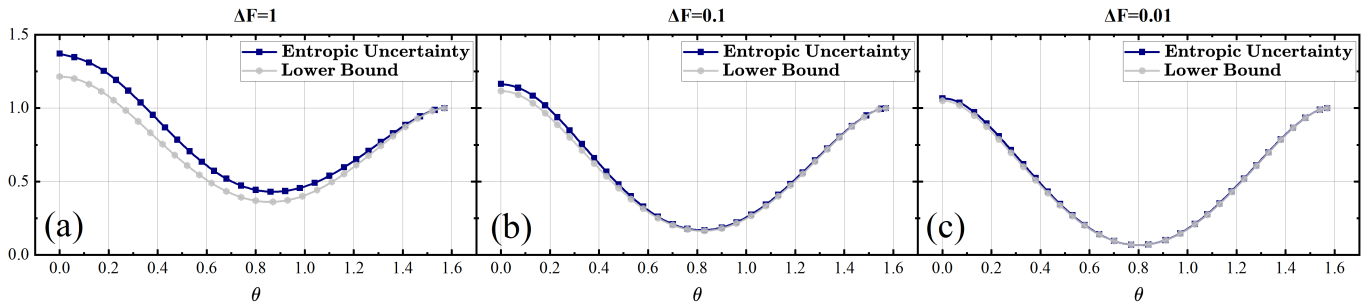


FIG. 8. Uncertainty and lower bound with the state's parameter θ for various ΔF in Graphs (a)–(c). Graph (a): $\Delta F = 1$, Graph (b): $\Delta F = 0.1$, and Graph (c): $\Delta F = 0.01$, where $c = d = m = 1$.

$S(\hat{\rho}_B)$ represent the von Neumann entropies of the post-measurement states. Consequently, the quantum states can be expressed as:

$$\begin{aligned}\hat{\rho}_{\hat{X}B} &= \sum_i (|x_i\rangle\langle x_i| \otimes \hat{\mathbb{I}}) \hat{\rho}_{AB} (|x_i\rangle\langle x_i| \otimes \hat{\mathbb{I}}), \\ \hat{\rho}_{\hat{Z}B} &= \sum_i (|z_i\rangle\langle z_i| \otimes \hat{\mathbb{I}}) \hat{\rho}_{AB} (|z_i\rangle\langle z_i| \otimes \hat{\mathbb{I}}),\end{aligned}\quad (25)$$

after performing two Pauli measurements, \hat{X} and \hat{Z} , where $\hat{\mathbb{I}}$ is the identity matrix, and $|x_i\rangle$ and $|z_i\rangle$ are the eigenvectors of the corresponding Pauli matrices. Significant progress has been made in the study of QMA-EUR. To better understand QMA-EUR, we consider an uncertainty game between two legitimate players, Alice and Bob. The results obtained were in agreement. In two measurements, \hat{R} and \hat{S} , one of the players, say Bob, prepares two particles, A and B in an entangled state. Then, Bob sends particle A to Player Alice while keeping B as quantum memory. Subsequently, Alice selects either \hat{R} or \hat{S} for measurement and records the outcome. She then communicates her measurement choice to Bob via a classical channel. Bob's task is to predict Alice's result with minimal uncertainty, which is constrained by Eq. (24). To be explicit, the entropic uncertainty and its lower bound in the current model have been derived, as detailed in Appendix D.

Fig. 8(a)–(c) depicts the entropic uncertainty and its lower bound with θ for different energy ratios ΔF . As observed in the figures, the entropic uncertainty initially decreases and then increases to a fixed value with increasing parameter θ . Notably, the uncertainty is strongly anticorrelated with quantum coherence, as shown in Fig. 3. Interestingly, the analysis reveals that a smaller energy ratio ΔF results in a tighter bound, meaning that the difference between the uncertainty and its lower bound decreases. This suggests that, for relatively small ΔF , the bound effectively captures the uncertainty, as further illustrated in Fig. 8. Additionally, the decline in quantum resources mentioned above can be attributed to the interaction between the detector and the environment, which reduces the system's purity. From an entropy perspective, the loss of information within the system increases its uncertainty, implying that less information can be extracted from the system of interest. Consequently, this study provides a promising new perspective for quantifying the quantumness

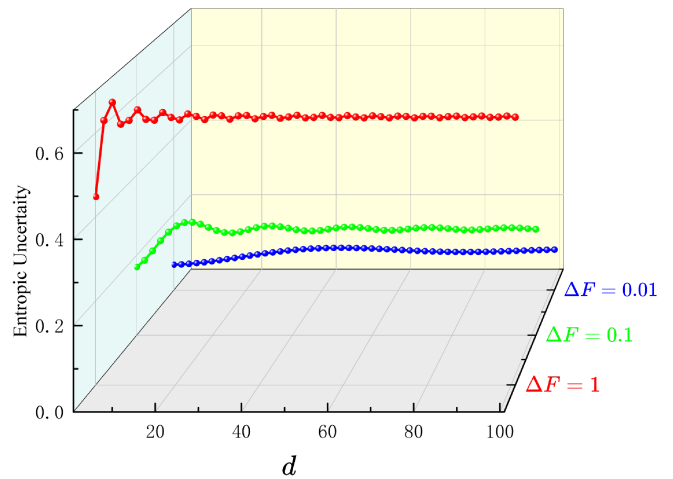


FIG. 9. Uncertainty with the distance between two detectors, with the energy ratio set as $\Delta F = 1$ (red), $\Delta F = 0.1$ (green), and $\Delta F = 0.01$ (blue), where $c = m = 1$.

of the system.

Finally, we explore how the distance d between the two detectors influences the evolution of entropic uncertainty. As depicted in Fig. 9, the uncertainty exhibits oscillatory growth as the distance d increases, and eventually stabilizes at a fixed value when the detectors are sufficiently far apart, i.e., $d \rightarrow \infty$. This behavior can be attributed to the minimal quantumness of the system in this regime, as shown in Figs. 4 and 5, which results in maximal measurement uncertainty.

IV. CONCLUSION

In this work, we explored the dynamics of quantum non-locality, quantum coherence, the nonlocal advantage of quantum coherence, and measurement uncertainty within a relativistic framework. Specifically, we considered a pair of static Unruh-DeWitt detectors interacting independently with an external field. Our analysis revealed how state parameters, the energy ratio, and the distance between the detectors influence the quantumness of the system. Notably, several meaningful results were obtained: (i) A larger energy ratio reduces both

Bell nonlocality and quantum coherence in the Unruh-DeWitt detector system, with higher energy ratios ΔF degrading the system's quantumness. (ii) An increasing distance d between the detectors weakens both the l_1 -norm coherence and the relative entropy of coherence, eventually stabilizing at fixed values as the distance approaches infinity. (iii) Regarding the nonlocal advantage of coherence, the l_1 -norm coherence is more robust than the relative entropy of coherence within the relativistic framework. (iv) The measured uncertainty of the system is strongly correlated with nonlocality and quantum coherence. Overall, these findings provide deeper insights into the quantumness of a pair of static Unruh-DeWitt detec-

tors and hold fundamental significance for future quantum information processing in relativistic settings.

ACKNOWLEDGMENTS

This work was supported by the National Natural Science Foundation of China (Grant Nos. 12475009 and 12075001, and 62471001), Anhui Provincial Key Research and Development Plan (Grant No. 2022b13020004), Anhui Province Science and Technology Innovation Project (Grant No. 202423r06050004), and Anhui Provincial University Scientific Research Major Project (Grant No. 2024AH040008).

-
- [1] C. H. Bennett, G. Brassard, C. Crépeau, R. Jozsa, A. Peres, and W. K. Wootters, *Phys. Rev. Lett.* **70**, 1895 (1993).
- [2] T. Schreiber, *Phys. Rev. Lett.* **85**, 461 (2000).
- [3] R. Raussendorf and H. J. Briegel, *Phys. Rev. Lett.* **86**, 5188 (2001).
- [4] C. Nayak, S.H. Simon, A. Stern, M. Freedman, and S. Das-Sarma *Rev. Mod. Phys.* **80**, 1083 (2008).
- [5] J. S. Bell, *Physics Physique Fizika* **1**, 195 (1964).
- [6] H. M. Wiseman, S. J. Jones, and A. C. Doherty, *Phys. Rev. Lett.* **98**, 140402 (2007).
- [7] E. G. Cavalcanti, S. J. Jones, H. M. Wiseman, and M. D. Reid, *Phys. Rev. A* **80**, 032112 (2009).
- [8] S. P. Walborn, A. Salles, R. M. Gomes, F. Toscano, and P. H. Souto Ribeiro, *Phys. Rev. Lett.* **106**, 130402 (2011).
- [9] J. F. Clauser, M. A. Horne, A. Shimony, and R. A. Holt, *Phys. Rev. Lett.* **23**, 880 (1969).
- [10] A. Peres, *Phys. Rev. Lett.* **77**, 1413 (1996).
- [11] D. Barman, A. Choudhury, B. Kad, and B. R. Majhi, *Phys. Rev. D* **107**, 045001 (2023).
- [12] T. R. Bromley, M. Cianciaruso, and G. Adesso, *Phys. Rev. Lett.* **114**, 210401 (2015).
- [13] T. Baumgratz, M. Cramer, and M. B. Plenio, *Phys. Rev. Lett.* **113**, 140401 (2014).
- [14] A. Blais, R.-S. Huang, A. Wallraff, S. M. Girvin, and R. J. Schoelkopf, *Phys. Rev. A* **69**, 062320 (2004).
- [15] F. Shahandeh, A. P. Lund, and T. C. Ralph, *Phys. Rev. A* **99**, 052303 (2019).
- [16] S. Rana, P. Parashar, and M. Lewenstein, *Phys. Rev. A* **93**, 012110 (2016).
- [17] H.-L. Shi, S.-Y. Liu, X.-H. Wang, W.-L. Yang, Z.-Y. Yang, and H. Fan, *Phys. Rev. A* **95**, 032307 (2017).
- [18] S. Rana, P. Parashar, A. Winter, and M. Lewenstein, *Phys. Rev. A* **96**, 052336 (2017).
- [19] K. Bu, U. Singh, S.-M. Fei, A. K. Pati, and J. Wu, *Phys. Rev. Lett.* **119**, 150405 (2017).
- [20] R. Lecamwasam, S. Assad, J. J. Hope, P. K. Lam, J. Thompson, and M. Gu, *PRX Quantum* **5**, 030303 (2024).
- [21] D. Mondal, T. Pramanik, and A. K. Pati, *Phys. Rev. A* **95**, 010301 (2017).
- [22] M. A. Ballester and S. Wehner, *Phys. Rev. A* **75**, 022319 (2007).
- [23] A. K. Pati, M. M. Wilde, A. R. U. Devi, A. K. Rajagopal, and Sudha, *Phys. Rev. A* **86**, 042105 (2012).
- [24] T. Pramanik, S. Mal, and A. S. Majumdar, *Quantum Inf. Process.* **15**, 981 (2016).
- [25] M.-L. Hu and H. Fan, *Phys. Rev. A* **87**, 022314 (2013).
- [26] T. Pramanik, P. Chowdhury, and A. S. Majumdar, *Phys. Rev. Lett.* **110**, 020402 (2013).
- [27] P. J. Coles and M. Piani, *Phys. Rev. A* **89**, 022112 (2014).
- [28] Z.-A. Wang, B.-F. Xie, F. Ming, Y.-T. Wang, D. Wang, Y. Meng, Z.-H. Liu, K. Xu, J.-S. Tang, L. Ye, C.-F. Li, G.-C. Guo, and S. Kais, *Phys. Rev. A* **110**, 062220 (2024).
- [29] S. Zozor, G. M. Bosyk, and M. Portesi, *J. Phys. A: Math. Theor.* **47**, 495302 (2014).
- [30] S. Liu, L.-Z. Mu, and H. Fan, *Phys. Rev. A* **91**, 042133 (2015).
- [31] F. Adabi, S. Salimi, and S. Haseli, *Phys. Rev. A* **93**, 062123 (2016).
- [32] J.-L. Huang, W.-C. Gan, Y. Xiao, F.-W. Shu, and M.-H. Yung, *Eur. Phys. J. C* **78**, 545 (2018).
- [33] F. Ming, D. Wang, X.-G. Fan, W.-N. Shi, L. Ye, and J.-L. Chen, *Phys. Rev. A* **102**, 012206 (2020).
- [34] F. Ming, X.-K. Song, J. Ling, L. Ye, and D. Wang, *Eur. Phys. J. C* **80**, 275 (2020).
- [35] L. Wu, L. Ye, and D. Wang, *Phys. Rev. A* **106**, 062219 (2022).
- [36] M.-L. Song, L.-J. Li, X.-K. Song, L. Ye, and D. Wang, *Phys. Rev. E* **106**, 054107 (2022).
- [37] L.-J. Li, F. Ming, X.-K. Song, L. Ye, and D. Wang, *Eur. Phys. J. C* **82**, 726 (2022).
- [38] B.-F. Xie, F. Ming, D. Wang, L. Ye, and J.-L. Chen, *Phys. Rev. A* **104**, 062204 (2021).
- [39] L.-J. Li, F. Ming, X.-K. Song, L. Ye, and D. Wang, *Eur. Phys. J. C* **81**, 728 (2021).
- [40] Z.-Y. Ding, H. Yang, D. Wang, H. Yuan, J. Yang, and L. Ye, *Phys. Rev. A* **101**, 032101 (2020).
- [41] M.-L. Song, X.-K. Song, L. Ye, and D. Wang, *Phys. Rev. E* **109**, 064103 (2024).
- [42] T.-Y. Wang, D. Wang, *Phys. Lett. B* **855**, 138876 (2024).
- [43] P. Calabrese and J. Cardy, *J. Stat. Mech.: Theory Exp.* **2004**, P06002 (2004).
- [44] I. Fuentes-Schuller and R. B. Mann, *Phys. Rev. Lett.* **95**, 120404 (2005).
- [45] P. Calabrese, J. Cardy, and E. Tonni, *Phys. Rev. Lett.* **109**, 130502 (2012).
- [46] A. Almheiri, D. Marolf, J. Polchinski, and J. Sully, *J. High Energy Phys.* **2013**, 62 (2013).
- [47] S. W. Hawking, *Commun. Math. Phys.* **43**, 199 (1975).
- [48] D. Marolf, *Rep. Prog. Phys.* **80**, 092001 (2017).
- [49] B. Reznik, *Found. Phys.* **33**, 167 (2003).
- [50] S. J. Summers and R. Werner, *Phys. Lett. A* **110**, 257 (1985).
- [51] A. Valentini, *Phys. Lett. A* **153**, 321 (1991).
- [52] S. J. Summers and R. Werner, *J. Math. Phys.* **28**, 2440 (1987).

[53] B. Reznik, A. Retzker, and J. Silman, *Phys. Rev. A* **71**, 042104 (2005).

[54] D. Deutsch, *Phys. Rev. Lett.* **50**, 631 (1983).

[55] K. Kraus, *Phys. Rev. D* **35**, 3070 (1987).

[56] H. Maassen and J. B. M. Uffink, *Phys. Rev. Lett.* **60**, 1103 (1988).

Appendix A: Analytical results of Bell nonlocality

In the calculation above, we derived the final state $\hat{\rho}_{AB}$ of the entire system. Subsequently, by inserting matrix into Eq. (16), the maximum CHSH inequality violation can be explicitly expressed as:

$$B(\hat{\rho}_{AB}) = 2\sqrt{\frac{c\pi(\alpha^2 + \gamma^2) - \gamma^2 \text{Re}(\sqrt{\Delta F})}{c^2\pi^2} + \frac{\gamma^2 \left(-4cd\pi\alpha + d\alpha \text{Re}(\sqrt{\Delta F}) + c\gamma \sin\left(\frac{d \text{Re}(\sqrt{\Delta F})}{c}\right) \right)}{4c^2d^2\pi^2}}. \quad (\text{A1})$$

To enhance the interpretability of our results, we perform a normalization procedure on the above formula,

$$B_{\text{Norm}}(\hat{\rho}_{AB}) := \max \left\{ 0, \frac{B(\hat{\rho}_{AB}) - 2}{B_{\text{max}}(\hat{\rho}_{AB}) - 2} \right\}, \quad (\text{A2})$$

where $B_{\text{max}}(\hat{\rho}_{AB}) = 2\sqrt{2}$. Here, $\alpha = \sin \theta$ and $\gamma = \cos \theta$ are state parameters. Referring to Eq. (9) because the detectors are same, we obtain $P = P'_A/T = P'_B/T = \frac{\delta(0)}{2c^3T} \sqrt{\Delta F}$, and $\mathfrak{R}_{AB} = \mathfrak{R}_{AB}/T = \frac{\delta(0)}{2c^3/T} \sqrt{\Delta F} \frac{\sin(\frac{d}{c} \sqrt{\Delta F})}{(\frac{d}{c} \sqrt{\Delta F})}$.

Appendix B: Analytical results of l_1 -norm coherence and relative entropy of coherence

Resorting to Eq. (17), the l_1 -norm coherence is given by

$$C_{l_1}(\hat{\rho}_{AB}) = 2\alpha\gamma(1 - 2c^2M) + 2\gamma^2c^2\mathfrak{R}_{AB}, \quad (\text{B1})$$

where $M = \text{Re}(M_A)/T = \text{Re}(M_B)/T = \frac{\delta(0)}{4c^3T} \sqrt{\Delta F}$. When distance $d \rightarrow \infty$, the results of l_1 -norm coherence can be written as $C_{l_1}^{(d \rightarrow \infty)}(\hat{\rho}_{AB}) \simeq 2\alpha\gamma(1 - 2c^2M)$, is independent of the distance.

Resorting to Eq. (18), ρ is the final state; we consider $\hat{\rho}_{AB}(t)$ and $\hat{\rho}_{\text{diag}}$ as the incoherent states of $\hat{\rho}_{AB}(t)$, which can be written as follows:

$$\hat{\rho}_{AB}(t) = \begin{pmatrix} \rho_{11} & 0 & 0 & \rho_{14} \\ 0 & \rho_{22} & \rho_{23} & 0 \\ 0 & \rho_{32} & \rho_{33} & 0 \\ \rho_{41} & 0 & 0 & \rho_{44} \end{pmatrix}, \quad (\text{B2})$$

$$\hat{\rho}_{\text{diag}} = \begin{pmatrix} \rho_{11} & 0 & 0 & 0 \\ 0 & \rho_{22} & 0 & 0 \\ 0 & 0 & \rho_{33} & 0 \\ 0 & 0 & 0 & \rho_{44} \end{pmatrix}. \quad (\text{B3})$$

According to the von Neumann entropy $S(\hat{\rho}) = -\text{Tr}(\hat{\rho} \log \hat{\rho})$, the relative entropy of the coherence can be written as

$$C_{\text{REC}}(\hat{\rho}_{AB}) = - \sum_{i=1,2,3,4} \lambda_i \log_2(\lambda_i) + \sum_{k=1,2,3,4} \mu_k \log_2(\mu_k), \quad (\text{B4})$$

where $\lambda_i (i = 1, 2, 3, 4)$ are the eigenvalues of $\hat{\rho}$ and $\mu_k (k = 1, 2, 3, 4)$ are the eigenvalues of $\hat{\rho}_{\text{diag}}$; in detail, $\lambda_1 = \frac{\mathfrak{R} - \aleph}{4c^2d\pi}$, $\lambda_2 = \frac{\mathfrak{R} + \aleph}{4c^2d\pi}$, $\lambda_3 = \frac{\cos^2(\theta)(d \text{Re}(\sqrt{\Delta F}) - c \sin(d \text{Re}(\sqrt{\Delta F})/c))}{4cd\pi}$, $\lambda_4 = \frac{\cos^2(\theta)(d \text{Re}(\sqrt{\Delta F}) + c \sin(d \text{Re}(\sqrt{\Delta F})/c))}{4cd\pi}$

$$\mathfrak{R} := 2c^2d\pi - cd \cos^2(\theta) \text{Re}(\sqrt{\Delta F}), \quad \aleph := \sqrt{c^2d^2 \left(4c^2\pi^2 + \cos^2(\theta) \text{Re}(\sqrt{\Delta F}) \left(-4c\pi + \text{Re}(\sqrt{\Delta F}) \right) \right)}.$$

Moreover, when the distance $d \rightarrow \infty$, the eigenvalues are calculated as

$$\begin{aligned}\lambda_1(d \rightarrow \infty) &\simeq \frac{2c\pi - \cos^2(\theta)\text{Re}\sqrt{\Delta F} - \sqrt{(4c^2\pi^2 + \cos^2(\theta)\text{Re}(\sqrt{\Delta F})(-4c\pi + \text{Re}(\sqrt{\Delta F})))}}{4\pi}, \\ \lambda_2(d \rightarrow \infty) &\simeq \frac{2c\pi - \cos^2(\theta)\text{Re}\sqrt{\Delta F} + \sqrt{(4c^2\pi^2 + \cos^2(\theta)\text{Re}(\sqrt{\Delta F})(-4c\pi + \text{Re}(\sqrt{\Delta F})))}}{4\pi}, \\ \lambda_3(d \rightarrow \infty) = \lambda_4(d \rightarrow \infty) &\simeq \frac{\cos^2(\theta)\text{Re}\sqrt{\Delta F}}{4c\pi}.\end{aligned}\tag{B5}$$

Furthermore, $\mu_k (k = 1, 2, 3, 4)$ are the eigenvalues of $\hat{\rho}_{\text{diag}}$, and they are given by $\mu_1 = \frac{\cos^2(\theta)(2c\pi - \text{Re}(\sqrt{\Delta F}))}{2c\pi}$, $\mu_2 = \mu_3 = \frac{\cos^2(\theta)\text{Re}(\sqrt{\Delta F})}{4c\pi}$, $\mu_4 = \sin^2(\theta)$.

Appendix C: Analytical expressions of the nonlocal advantage of quantum coherence

By utilizing Eq. (20), the analytical result for nonlocal advantage of l_1 -norm coherence can be expressed as follows:

$$\begin{aligned}\mathcal{N}^{l_1}(\hat{\rho}_{AB}) &= \frac{4\pi c - 3\sqrt{\Delta F} \cos^2 \theta (\sqrt{\Delta F} + 4\pi c (\sec^2 \theta - 1))}{4\pi c (4\pi c - \sqrt{\Delta F})} \\ &+ \frac{\cos^2 \theta \left(c \cos \theta \sin\left(\frac{d\sqrt{\Delta F}}{c}\right) + d(-4\pi c + \sqrt{\Delta F} \sin \theta) \right)}{4\pi c d} \\ &+ \frac{(-4\pi c + \sqrt{\Delta F}) \cos^2 \theta (\sqrt{\Delta F} \cos^2 \theta - 4\pi c \sin^2 \theta)}{2c(-\pi(4\pi c + \sqrt{\Delta F}) + \pi(4\pi c - \sqrt{\Delta F}) \cos(2\theta))} \\ &+ \frac{\cos^2 \theta \left(c \sin\left(\frac{d\sqrt{\Delta F}}{c}\right) + d(4\pi c - \sqrt{\Delta F}) \tan \theta \right)}{4\pi c d} \\ &+ \frac{1}{2} \sqrt{\frac{\cos^2 \theta \left(c \cos \theta \sin\left(\frac{d\sqrt{\Delta F}}{c}\right) + d(-4\pi c + \sqrt{\Delta F}) \sin \theta \right)^2}{4\pi^2 c^2 d^2} + \left(\left(-1 + \frac{\sqrt{\Delta F}}{2\pi c} \cos^2 \theta \right) + \sin^2 \theta \right)^2} \\ &+ \frac{1}{2} \sqrt{\frac{\cos^4 \theta \left(c \sin\left(\frac{d\sqrt{\Delta F}}{c}\right) + d(4\pi c - \sqrt{\Delta F}) \tan \theta \right)^2}{4\pi^2 c^2 d^2} + \left(\left(-1 + \frac{\sqrt{\Delta F}}{2\pi c} \cos^2 \theta \right) + \sin^2 \theta \right)^2}.\end{aligned}\tag{C1}$$

Because the analytical results of nonlocal advantage of the REC are highly complex, we do not present them in this paper. To make the results more intuitive, we perform a normalization operation on the above formula, yielding the following results:

$$\mathcal{N}_{\text{Norm}}^{l_1}(\hat{\rho}_{AB}) := \max \left\{ 0, \frac{\mathcal{N}^{l_1}(\hat{\rho}_{AB}) - \sqrt{6}}{\mathcal{N}_{\text{max}}^{l_1}(\hat{\rho}_{AB}) - \sqrt{6}} \right\},\tag{C2}$$

$$\mathcal{N}_{\text{Norm}}^{\text{REC}}(\hat{\rho}_{AB}) := \max \left\{ 0, \frac{\mathcal{N}^{\text{REC}}(\hat{\rho}_{AB}) - 2.23}{\mathcal{N}_{\text{max}}^{\text{REC}}(\hat{\rho}_{AB}) - 2.23} \right\},\tag{C3}$$

where $\mathcal{N}_{\text{max}}^{l_1}(\hat{\rho}_{AB}) = \mathcal{N}_{\text{max}}^{\text{REC}}(\hat{\rho}_{AB}) = 3$.

Appendix D: Analytical expressions of the entropic uncertainty and lower bound

To compute the uncertainty and its lower bound, which correspond to the left and right sides of Eq. (24), we consider the state of the system after measurements with the two incompatible observables $\hat{\sigma}_x$ and $\hat{\sigma}_z$, as follows:

$$\hat{\rho}_{\hat{X}B} = \begin{pmatrix} \frac{\rho_{11}+\rho_{33}}{2} & 0 & 0 & \frac{\rho_{14}+\rho_{32}}{2} \\ 0 & \frac{\rho_{22}+\rho_{44}}{2} & \frac{\rho_{23}+\rho_{41}}{2} & 0 \\ 0 & \frac{\rho_{14}+\rho_{32}}{2} & \frac{\rho_{11}+\rho_{33}}{2} & 0 \\ \frac{\rho_{23}+\rho_{41}}{2} & 0 & 0 & \frac{\rho_{22}+\rho_{44}}{2} \end{pmatrix}, \quad (\text{D1})$$

$$\hat{\rho}_{\hat{Z}B} = \begin{pmatrix} \rho_{11} & 0 & 0 & 0 \\ 0 & \rho_{22} & 0 & 0 \\ 0 & 0 & \rho_{33} & 0 \\ 0 & 0 & 0 & \rho_{44} \end{pmatrix}. \quad (\text{D2})$$

Furthermore, the reduced density matrix of Bob's detector can be expressed as:

$$\hat{\rho}_B = \begin{pmatrix} \rho_{11} + \rho_{33} & 0 \\ 0 & \rho_{22} + \rho_{44} \end{pmatrix}, \quad (\text{D3})$$

by tracing out the degrees of freedom of Alice's detector. The explicit expression for the entropic uncertainty is then given by

$$S(\hat{X}|B) + S(\hat{Z}|B) = -\sum_i \lambda_i \log_2(\lambda_i) - \sum_i \epsilon_i \log_2(\epsilon_i) + 2 \sum_k \mu_k \log_2(\mu_k), \quad (\text{D4})$$

where $\lambda_1 = \lambda_2 = \frac{1}{4}(1 - \Gamma)$; $\lambda_3 = \lambda_4 = \frac{1}{4}(1 + \Gamma)$ are the eigenvalues of the matrix $\hat{\rho}_{\hat{X}B}$ with $\Gamma = \sqrt{\alpha^4 + 2(1 + 2c^2(4M(-1 + c^2M) + P))\alpha^2\gamma^2 + 8c^2(1 - 2c^2M)\Re_{AB}\alpha\gamma^3 + ((1 - 2c^2P)^2 + 4c^4\Re_{AB}^2)\gamma^4}$, $\epsilon_1 = (1 - 2c^2P)\gamma^2$, $\epsilon_2 = \epsilon_3 = \gamma^2 c^2 P$ and $\epsilon_4 = \alpha^2$ are the eigenvalues of the matrix $\hat{\rho}_{\hat{Z}B}$, and $\mu_1 = (1 - c^2P)\gamma^2$ and $\mu_2 = \alpha + c^2P\gamma^2$ are the eigenvalues of $\hat{\rho}_B$.

Additionally, the lower bound of uncertainty can be written as:

$$q_{MU} + S(A|B) = 1 + \left(-\sum_{i=1}^4 \zeta_i \log_2(\zeta_i) + \sum_{k=1}^2 \mu_k \log_2(\mu_k) \right), \quad (\text{D5})$$

where $\{\zeta_i | i = 1, 2, 3, 4\}$ is the eigenvalue of the matrix $\hat{\rho}_{AB}$, and it can be expressed by

$$\begin{aligned} \zeta_1 &= c^2(P - \Re_{AB})\gamma^2, \\ \zeta_2 &= c^2(P + \Re_{AB})\gamma^2, \\ \zeta_3 &= \frac{1}{2}(\alpha^2 + (1 - 2c^2P)\gamma^2 - \Xi), \\ \zeta_4 &= \frac{1}{2}(\alpha^2 + (1 - 2c^2P)\gamma^2 + \Xi) \end{aligned}$$

with $\Xi = \sqrt{(\alpha^4 + 2(1 + 2c^2(4M(-1 + c^2M) + P))\alpha^2\gamma^2 + (1 - 2c^2P)^2\gamma^4)}$.